RSC Advances

PAPER

View Article Online
View Journal | View Issue

Cite this: *RSC Adv.*, 2017, **7**, 30221

Impact of size control of graphene oxide nanosheets for enhancing electrical and mechanical properties of carbon nanotube–polymer composites†

Jeonghwan Kim, Sang Woo Kim, Hongseok Yun* and Bumjoon J. Kim*

Graphene oxide (GO) has been explored for improving the dispersion stability of carbon nanotubes (CNTs). In particular, the size and shape of GO sheets have a significant impact on determining their dispersion efficiency and optimizing the properties of the CNT-based composites, but, to date, such effects have never been systematically assessed. In this study, we evaluated the size effects of GOs on the dispersion behavior of multi-walled CNTs (MWCNTs), and exploited them to develop conducting film and polymer–CNT composites with excellent electrical and mechanical properties. Synthesis of a series of five different GOs with varied sizes ranging from 170 to 2060 nm, but nearly the same surface properties, allowed systematical investigation of size effects of GO sheets. The CNT-dispersing ability of the GOs was improved significantly as the size of the sheets decreased. For example, the critical GO-to-MWCNT ratio (W_{GO}/W_{MWCNT}) required to produce stable MWCNT dispersion was in proportion to the size of the GO. Furthermore, the minimum value of the W_{GO}/W_{MWCNT} ratio required to fabricate a conductive GO–MWCNT film underwent a dramatic decrease from 0.1 to 0.025 as the size of the GO sheets changed from 2060 to 170 nm. Small-sized GOs facilitated the formation of an interconnected MWCNT network more effectively than large-sized GOs. Further investigation of the size effects of the GO on the mechanical properties of polymer–MWCNT composites was performed by measuring the Young's modulus of the composites. A two-fold enhancement in the mechanical properties of the polymer–CNT composites was achieved by controlling the size of GO. Our results provide important guidelines for the design of carbonaceous-material-based composites with excellent electrical and mechanical properties.

Received 9th April 2017
Accepted 26th May 2017

DOI: 10.1039/c7ra04015f

rsc.li/rsc-advances

Introduction

Carbon nanotube (CNT)–polymer nanocomposite materials have shown great potential in various applications including structural composite materials,[1–4] energy storage devices,[5–9] and transparent electrodes.[10–13] However, the potential of employing CNT-based nanocomposites has been limited mainly by their strong tendency to agglomerate in solvents or in polymer matrices through strong van der Waals interaction, thereby restricting the compatibility of the CNTs with other functional materials.[14–17] In this regard, a great deal of research has been devoted to preventing CNT agglomeration and improving the dispersion quality of CNTs.[18–21] Although several methods using chemical functionalization or organic surfactants have been suggested for exfoliating CNTs in solvent, such methods often suffer from degradation of electrical and mechanical properties of CNTs due to the formation of defects on the surfaces of the CNTs or the insulating nature of the surfactants. Recently, graphene oxide (GO) has received much attention as a platform for many applications in aqueous media, such as pH, thermal, and optical sensors, due to its amphiphilic structure, which consists of a hydrophobic, π-conjugated 2D carbon sheet that contains various hydrophilic oxygen functional groups.[22–31] In particular, the strong chemical affinity of GO for CNT *via* non-destructive π–π interactions facilitates the use of GO as a surfactant for CNTs.[30,32–37] However, the dispersing efficiency of GO was often limited due to the large size of two-dimensional GO, *i.e.*, typically greater than a micrometer, which produces mismatches with the sizes of the CNTs. Therefore, the ability to engineer the size of GO at the nanoscale (*i.e.*, graphene quantum dot) can provide a powerful strategy to improve the dispersion stability of the CNTs owing to the high surface-to-volume ratio of nano-sized GOs compared with those of micron-sized GO sheets.[38–43] Importantly, the size effects of GO on CNT dispersion stability as well as the electrical and mechanical properties of CNT-based nanocomposites have

Department of Chemical and Biomolecular Engineering, Korea Advanced Institute of Science and Technology (KAIST), Daejeon 34141, Republic of Korea. E-mail: bumjoonkim@kaist.ac.kr; hongsyun@kaist.ac.kr

† Electronic supplementary information (ESI) available: The additional characterization data of GOs and MWCNTs, including TEM, SEM, AFM, ATR-FTIR, XPS and UV-vis absorption spectroscopy. See DOI: 10.1039/c7ra04015f

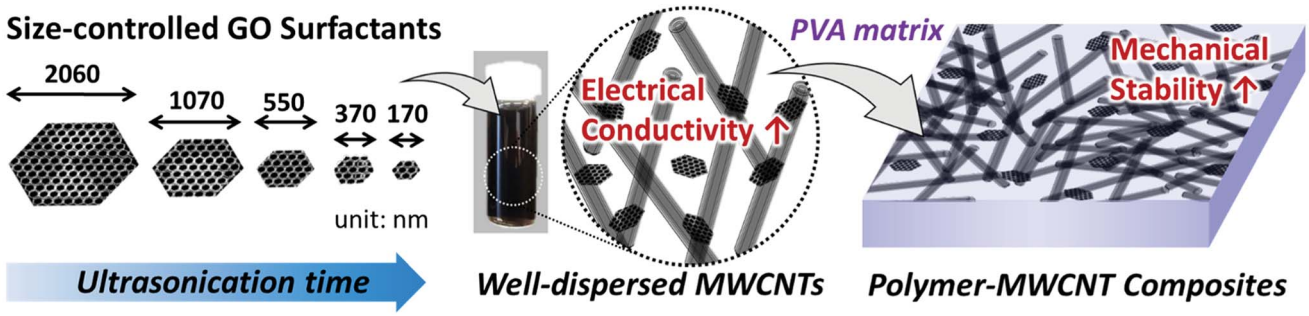

Scheme 1 Schematic illustration of the preparation of size-controlled GO nanosheets through an ultrasonication process, and their application in the conductive GO–MWCNT film and PVA–MWCNT composites with excellent electrical and mechanical properties.

never been assessed. Thus, it is of great importance to systematically evaluate the size dependence of the dispersing ability of GO sheets in order to optimize the electrical and mechanical properties of CNT-composite materials.

In this work, we synthesized a series of size-controlled GOs to investigate the size effects of the GOs on the dispersion of multi-walled CNTs (MWCNTs) (Scheme 1), and demonstrated their impact on the electrical and mechanical properties of MWCNT composites. Ultrasonication was used to prepare GOs with nearly identical surface properties with lateral sizes ranging from 170 to 2060 nm. The critical GO-to-MWCNT ratio (W_{GO}/W_{MWCNT}) required to achieve a stable dispersion of MWCNTs clearly depended on the size of the GOs, *i.e.*, the ratios were 0.83 for the 2060 nm GOs, and 0.14 for the 170 nm GOs, respectively. Further evaluation of the electrical properties of GO–MWCNT dispersions was performed by measuring the sheet resistance of MWCNT thin films. As the size of the GOs decreased from 2060 to 170 nm, the minimum W_{GO}/W_{MWCNT} value for fabricating conductive GO–MWCNT films was significantly reduced from 0.1 to 0.025. Finally, well-dispersed GO–MWCNTs were used as fillers to enhance the mechanical properties of the poly(vinyl alcohol) (PVA)-based composites, showing a reinforcement effect of the smallest GO (170 nm) two-fold greater than that of the largest GO (2060 nm).

Experimental

Materials

Graphite powder (particle size < 20 μm), MWCNTs (purity ≥98% carbon basis, outer diameter 6–13 nm, length about 2.5–20 μm), phosphoric acid (H_3PO_4), and PVA (MW 89 000–98 000, 99% hydrolyzed) were all purchased from Sigma-Aldrich. Sulfuric acid (H_2SO_4) was obtained from Samchun Chemical Co. Potassium permanganate ($KMnO_4$, 99%) was purchased from Junsei. All of the materials were used as-received without further purification.

Preparation of GO sheets

GO was synthesized from graphite powder by modifying a previously reported method.[44] First, 3 g of graphite flakes was added to a mixture of H_2SO_4/H_3PO_4 (360 : 40 mL). After allowing the reaction to proceed under ambient conditions for 2 h, 18 g of $KMnO_4$ was gradually added to the graphite solution. The solution was then heated to 50 °C, and stirred for 2 weeks. Then, the mixture was centrifuged and washed sequentially with deionized (DI) water, 10% HCl aqueous solution, and ethanol. The washing process was repeated several times. The remaining solvent was evaporated under vacuum, and purified GO was obtained.

To prepare size-controlled GOs, 500 mg of as-synthesized GO powders was dissolved in 50 mL of DI water and divided into five 20 mL vials. Then, each GO suspension (10 mg mL^{-1} in DI water) was subjected to ultrasonication using a probe type sonicator (Sonics Vibra-Cell VCX-500, 500 W, 20 kHz) at 25% amplitude for 0, 10, 30, 60, and 120 min to yield GO sheets with varied sizes. An ice bath was used to avoid increase in temperature during the probe sonication.

Preparation of GO–MWCNT dispersions in DI water

For a typical preparation of MWCNT stabilized by GO (GO–MWCNT) in DI water, a GO suspension in DI water (10 mg mL^{-1}) was added to a vial preloaded with MWCNTs (1 mg) to make a GO–MWCNT dispersion in DI water with a concentration of 0.1 mg mL^{-1}. The weight ratio of GO-to-MWCNT (W_{GO}/W_{MWCNT}) was varied from 1 : 50 to 1 : 1 to study its influence on the dispersibility. The mixtures were then subjected to probe sonication (Sonics Vibra-Cell VCX-500, 500 W, 20 kHz) for 1 min, and allowed to settle for 24 h.

Fabrication of GO–MWCNT papers

For the sheet resistance measurement, GO–MWCNT papers were fabricated by vacuum filtration of GO–MWCNT dispersion through a polymer membrane filter (Mixed Cellulose Ester membrane, 47 mm in diameter, 0.2 μm pore size, Hyundai Micro Co.). The sheet resistance of GO–MWCNT thin film was measured from the current–voltage behavior using a Keithley 2400 Source Measurement Unit. The reported data were the averages of five tests for each sample.

Preparation of PVA composite films

The PVA composite films were produced by the solution casting method.[45–48] Sixty grams of PVA powder was dissolved in DI water (400 mL) at 90 °C under stirring until the polymer was

completely dispersed. Then, the polymer solution was cooled down to room temperature. Subsequently, the prepared GO–MWCNT dispersions with different W_{GO}/W_{MWCNT} were each added into 10 mL PVA solution, and the resulting mixtures were stirred for 1 h to obtain homogeneous solutions. Then 20 mL of each solution was poured into a rectangular polymer Petri-dish, and desiccated at room temperature for 12 h, followed by annealing at 70 °C for 30 min. High quality transparent films with uniform surface were thus obtained with thicknesses of up to 0.3 mm. The thickness of the film was controlled mainly by the mass of PVA and the dimension of the Petri-dishes.

Characterization

Field emission scanning electron microscopy (FE-SEM, Hitachi S-4800) and transmission electron microscopy (TEM, JEOL 2000FX) analysis were performed to investigate the morphologies of GO and GO–MWCNT. TEM samples were prepared by dropping aqueous suspensions of GOs onto Cu grids coated with a holey carbon film followed by solvent evaporation under vacuum. The surface properties of GO sheets were characterized by attenuated total reflection Fourier-transform infrared (ATR-FTIR) spectroscopy using a Bruker ALPHA and X-ray photoelectron spectrometer (XPS, Thermo VG Scientific ESCA 2000). Atomic force microscopy (AFM) images and thickness profiles were measured using a Veeco Dimension 3100 instrument. The GO samples for SEM and AFM analyses were prepared by a dip-coating method on precleaned silicon substrate. UV-visible (UV-vis) absorption spectra were measured from diluted solutions (by a factor of 5–20 from 0.1 mg mL^{-1} suspensions) in DI water using a 1 cm path length quartz cuvette in a UV-1800 spectrophotometer (Shimadzu Scientific Instruments) at room temperature. The absorbance value at 500 nm of each GO–MWCNT sample was determined by subtracting the absorbance of GO from that of GO–MWCNT in order to exclude the influence of the GO on the resulting absorbance of MWCNT dispersed in the water.

The tensile behavior of PVA composite films was measured using an Instron 3343 tensile tester with the 1 kN load cell. All samples were cut from a flat sheet into strips of 70 mm × 12.5 mm × 0.3 mm. Uniaxial tensile testing was performed at a loading rate of 50 mm min^{-1} with a gauge length of 25 mm for each specimen.

Results and discussion

Size-controlled GO nanosheets

In order to investigate the size effect of GO sheets on the dispersing efficiency of the MWCNTs, a series of GO samples with varied lateral sizes but the same surface properties was prepared through breakdown of a parent GO sample, which was made from graphite powder following a previously reported chemical oxidation method.[44] Fig. 1(a)–(c) shows the SEM images of the GOs with different sizes. The average size of the parent GO (GO0) was determined to be 2060 nm by the SEM images. Then, the parent GOs were sonicated for 10, 30, 60, and 120 minutes, and the resulting samples were denoted GO1, GO2, GO3, and GO4, respectively. The sonication process broke down the as-synthesized GOs, yielding reduced average size of GO sheets: 1070 (GO1), 550 (GO2), 370 (GO3), and 170 (GO4) nm, as determined by the statistical analysis of the SEM images (see Fig. 1, S1† and Table 1). Fig. 1(d) shows that, overall, the size of the GO sheets decreased exponentially as a function of the ultrasonication processing time. The thicknesses of GOs were measured by AFM analysis, as shown in Fig. S2.† The average thicknesses were 16.5, 5.4, 5.4, 5.5, and 4.6 nm for GO0, GO1, GO2, GO3, and GO4, respectively. During the initial stage of sonication (10 min), the thickness of the GO decreased significantly from 16.5 nm (GO0) to 5.4 nm (GO1). However, GO1–GO4 exhibited similar thicknesses (~5 nm), indicating that the GO sheets were composed of a few layers and that additional sonication did not affect the thickness of the GO.

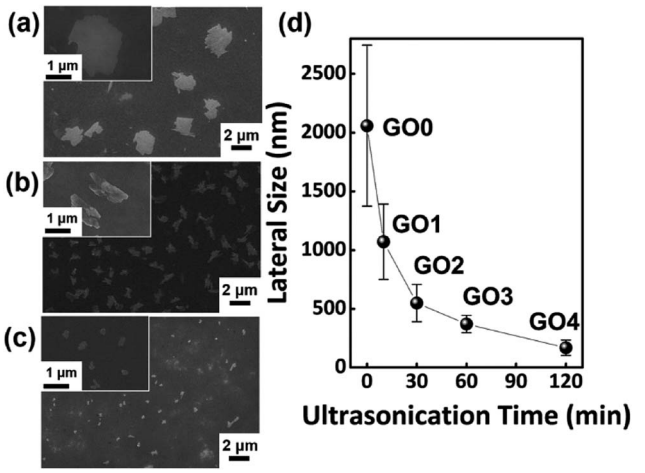

Fig. 1 SEM images of the size-controlled GOs subjected to different ultrasonication times: (a) 0 min (GO0), (b) 30 min (GO2), and (c) 120 min (GO4). (d) Average lateral sizes of GOs as a function of ultrasonication time.

FTIR spectroscopy and XPS measurements were carried out to determine the surface properties of the GOs. Fig. 2(a) shows that all of the GO samples had the broad and intense peak of O–OH group centered at 3400 cm^{-1} as well as the C=O stretching vibration peak at 1740 cm^{-1}. Also, they had the skeletal vibrations of the unoxidized graphitic C=C domains at 1620 cm^{-1},

Table 1 Average sizes of graphite and GOs with different sonication times

Samples	Ultrasonication time (min)	Avg. particle size[a] (nm)	Avg. layer thickness[b] (nm)
Graphite	—	8960 ± 3690	—
GO0	No sonication	2060 ± 690	16.5 ± 3.1
GO1	10	1070 ± 320	5.4 ± 0.4
GO2	30	550 ± 160	5.4 ± 0.6
GO3	60	370 ± 70	5.5 ± 0.9
GO4	120	170 ± 70	4.6 ± 1.1

[a] Measured as the mean diameter of the equivalent circular area from SEM images. [b] Measured from the height profiles of AFM images.

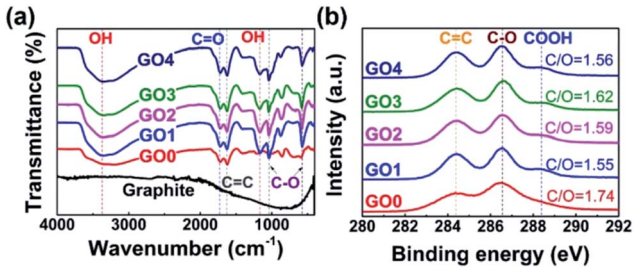

Fig. 2 Surface properties of size-controlled GOs: (a) FTIR spectra and (b) XPS C 1s spectra of graphite, GO0, GO1, GO2, GO3, and GO4.

the C–OH stretching vibration peak at 1220 cm^{-1}, and the C–O stretch of the COOH group at 1050 cm^{-1}. All of the GO samples showed almost identical band profiles, which were completely distinct from the profile of the precursor (*i.e.* graphite) owing to the formation of oxygen functional groups on the GO surface. Moreover, as shown in Fig. 2(b), XPS data also displayed analogous profiles for all of the GO samples, which were well superimposed on each other (Fig. S3†), with characteristic peaks at 284.4, 286.5, and 288.2 eV, representing C–C/C=C, C–O, and O=C–OH groups, respectively. The XPS data showed that the GOs had very similar C/O ratios in the range from 1.55 to 1.74, irrespective of the sonication time. The FTIR and XPS results confirmed that the different-sized GO samples possessed both sp^2 carbons and oxygen functional groups, both of which are essential for generating the π–π interactions with the MWCNTs and dipole–dipole interactions with the polar solvent (*i.e.*, water). Taken together, these characterization data demonstrated that the GO samples used in this study had comparable physicochemical surface properties but different lateral sizes, which made them suitable for assessing the effects of the size of the GO on the properties of GO–CNT composites.

GO–MWCNT dispersion

Next, the GO samples were tested as dispersants for MWCNTs. Two different dispersion states of the MWCNTs were observed from the photographic images in Fig. S4.† The pristine MWCNTs (Fig. S4(a)†) produced aggregates in DI water due to strong van der Waals interactions between individual MWCNTs, whereas the GO4–MWCNTs (Fig. S4(c)†) were dispersed well in DI water. In the TEM images, the pristine MWCNTs were severely agglomerated into micron-sized bundles (Fig. S4(b)†), whereas the GO–MWCNTs were well separated into thin, nano-sized fibrils (Fig. S4(d)†). These observations indicated that the hydrophobic basal planes of the GOs were successfully bound to the surface of the MWCNTs through π–π stacking interactions, separating the MWCNTs from each other and increasing the dispersion quality of the MWCNTs in solution.[49] In addition, the hydrophilic oxygen-containing groups on the edge of the GOs[32,33,50] facilitated the stabilization of the GO–MWCNTs through dipole–dipole interactions with water.

Next, the dispersion efficiency of MWCNTs was estimated by measuring the UV-vis absorbance of the GO–MWCNTs in water. For convenience, we defined the degree of MWCNT dispersion, D_{MWCNT}, as the ratio of the dispersed MWCNTs to the MWCNTs that were added to the solution initially. The concentration of the MWCNTs dispersed in water can be determined by the Beer's law equation, $A = \varepsilon \times L \times C$, where A is the absorbance of the MWCNT dispersion in water, ε is the extinction coefficient of the MWCNTs, L is the path length of the cuvette through which light passes, and C is the concentration of the dispersed MWCNTs in water. For example, the A values of GO4–MWCNT in solution were measured at different W_{GO}/W_{MWCNT} ratios. To determine the precise ε value for our MWCNTs, we measured the A values of the GO–MWCNT solutions at different wavelengths (500, 600 and 700 nm). Assuming that (1) the ratios of $A_{500\ nm}$, $A_{600\ nm}$, and $A_{700\ nm}$ are fixed for a given value of C (as shown in Fig. S5(a)†) and (2) A is linearly proportional to C, we performed the alternating least squares method for the dataset at different wavelengths to determine the values of $\varepsilon_{500\ nm}$, $\varepsilon_{600\ nm}$ and $\varepsilon_{700\ nm}$, which are shown in Fig. S5(b).† We obtained $\varepsilon_{500\ nm} = 37.2$ mL mg^{-1} cm^{-1}, which was in good agreements with the $\varepsilon_{500\ nm}$ values for other MWCNTs.[51–54] The C values of the GO4–MWCNT samples for different W_{GO}/W_{MWCNT} were calculated by normalizing them by the initially added amount of MWCNTs to produce D_{MWCNT} (Fig. 3).

The D_{MWCNT} values are plotted as a function of W_{GO}/W_{MWCNT} as presented in Fig. 3(a). All of the GO samples except GO0 exhibited similar hyperbolic profiles in their D_{MWCNT} curves where the D_{MWCNT} values increased sharply in proportion to W_{GO}/W_{MWCNT} at relatively low W_{GO}/W_{MWCNT} values (≤0.2), and the D_{MWCNT} values appeared to reach a plateau as the ratio was further increased to more than 0.5. However, the D_{MWCNT} values varied significantly from each other according to the size of GO. For example, at the W_{GO}/W_{MWCNT} of 0.1, the D_{MWCNT} values were 0.2, 0.7, 25.6, 33.5, and 47.0% for GO0, GO1, GO2, GO3, and GO4, respectively, which shows a dramatic increase of D_{MWCNT} upon decreasing the size of GO. In particular, over the whole range of W_{GO}/W_{MWCNT} that was measured in this study, the D_{MWCNT} values were ranked in the same order as the sizes of the GO. Fig. 3(b) shows that, when the W_{GO}/W_{MWCNT} increased further to over 0.5, each GO exhibited its own maximum value, D_{max}, *i.e.*, 52.3, 61.9, 72.0, 77.5, and 81.1% for GO0, GO1, GO2, GO3, and GO4, respectively. These results indicated that both the dispersing efficiency and the maximum dispersing ability of GOs were greatly enhanced by reducing the size of GO.

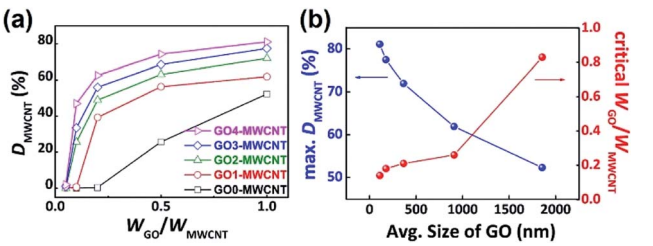

Fig. 3 (a) D_{MWCNT} as a function of W_{GO}/W_{MWCNT}, and (b) variations of the maximum D_{MWCNT} value and the critical W_{GO}/W_{MWCNT} as a function of the GO size. UV-vis measurements of all specimens were performed after a 24 h settling period.

Based on the data in Fig. 3(a), the critical W_{GO}/W_{MWCNT} ratios are calculated using linear regression statistics[53] and plotted as a function of GO size in Fig. 3(b). This term represents the minimum amount of GOs required to stabilize MWCNTs effectively, and, thus, lower critical W_{GO}/W_{MWCNT} indicates the more efficient dispersing ability of the GOs. Thus, the smaller GOs stabilized the MWCNTs more effectively than the larger GOs. For instance, the critical GO-to-MWCNT ratio values were significantly reduced from 0.83 to 0.14 as the size of the GOs decreased from 2060 nm (GO0) to 170 nm (GO4). These results were attributed to the fact that, at a fixed amount of GO, small-sized GOs have a larger number of sheets available for interaction with MWCNTs than large-sized GOs, therefore yielding better dispersion efficiency at a given value of W_{GO}/W_{MWCNT}.

Electrical properties of GO–MWCNT films

Next, we investigated the size effect of the GOs on the electrical properties of the MWCNT by evaluating the sheet resistances of MWCNT thin films. For the voltage–current measurements, GO–MWCNT films (Fig. S6†) were prepared by vacuum filtration of a GO–MWCNT dispersion (0.2 mg mL^{-1}) through a polymer membrane filter (pore size of 0.2 μm). As displayed in Fig. 4, staircase-like curves were obtained from all of the GO samples; the sheet resistance dropped suddenly at certain W_{GO}/W_{MWCNT} ratios, which were remarkably varied depending on the size of the GO. For example, at the W_{GO}/W_{MWCNT} of 0.02, the sheet resistances of all samples were higher than 10^{11} Ω sq^{-1}, indicating that all of the GO–MWCNT films were nearly insulating at this W_{GO}/W_{MWCNT}. When the W_{GO}/W_{MWCNT} ratio was increased to 0.025, the GO3–MWCNT and GO4–MWCNT films had drastically reduced sheet resistances, *i.e.*, 3.3×10^6 and 2.2×10^5 Ω sq^{-1}, respectively. By contrast, the sheet resistances of the GO1– and the GO2–MWCNT films became comparable to those of the GO3– and the GO4–MWCNT films only after the W_{GO}/W_{MWCNT} was increased to above 0.05. In a striking contrast, the GO0–MWCNT showed notably worse electrical performance compared with the other GO–MWCNT samples, and it required a W_{GO}/W_{MWCNT} ratio of 0.1 to lower the sheet resistance to less than 10^6 Ω sq^{-1}. Accordingly, the electrical properties of the GO–MWCNT composite were strongly dependent on the size of GO. This was evidenced by the fact that the minimum W_{GO}/W_{MWCNT} value required to build a conductive MWCNT film reduced progressively as the size of the GO decreased: 0.1 for GO0, 0.05 for GO1 and GO2, and 0.025 for GO3 and GO4.

Such GO size-dependent electrical properties of the GO–MWCNT films can be associated with the dependence of the quality of MWCNT dispersion on the size of the GOs. As evidenced in Fig. 3, the small-sized GOs exfoliate MWCNT bundles more effectively than large-sized GOs. Therefore, the small-sized GOs can help to achieve more evenly distributed MWCNTs, and thereby effectively form interconnected MWCNT networks, as supported by the SEM images in Fig. S6,† leading to a significantly lower W_{GO}/W_{MWCNT} required for fabricating conductive films. It is worth noting that there is a discrepancy between the critical W_{GO}/W_{MWCNT} for achieving stable dispersion and a conductive film. For example, in the case of GO4, the critical W_{GO}/W_{MWCNT} based on UV-vis data was 0.14, whereas the ratio from the sheet resistance data was 0.025; this difference was attributed to the differences between solid-state and liquid-state dispersion.

Mechanical properties of polymer–CNT composite films

CNTs have been investigated as reinforcing fillers for enhancing the mechanical stability of polymer composites, but one of the major hurdles to achieve this goal is the poor dispersion of the CNTs in solid matrices.[55–61] It was known that the uniform dispersion of the filler is one of the keys to effectively enhancing the physical properties of polymer composites.[62–68] Thus, we assessed the size effects of GO on the dispersion of GO–MWCNTs in the polymer matrix and the mechanical properties of polymer–MWCNT composites. The effect of GO-assisted CNTs on the mechanical properties of polymer matrices has been studied using PVA as a matrix.[46,47,69] PVA–MWCNT composites were prepared using GO0–, GO2–, and GO4–MWCNT as fillers, representing large-sized (2060 nm), medium-sized (550 nm), and small-sized (170 nm) GOs, respectively. The Young's moduli of the PVA–MWCNT composites were determined from their stress–strain curves (Fig. S7†) and plotted as a function of W_{GO}/W_{MWCNT} from 0 (*i.e.*, pristine MWCNT) to 1 at an MWCNT volume fraction of 1.2% where the differences between the samples emerged. The mechanical property data of

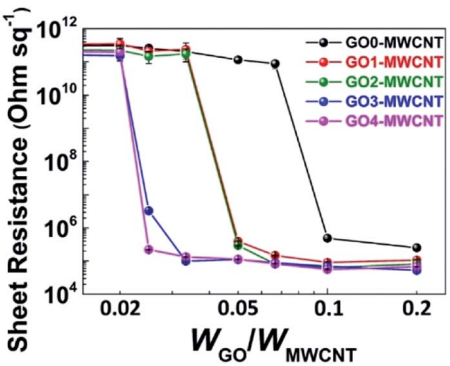

Fig. 4 Sheet resistances of thin films made from MWCNT suspensions stabilized by different-sized GOs.

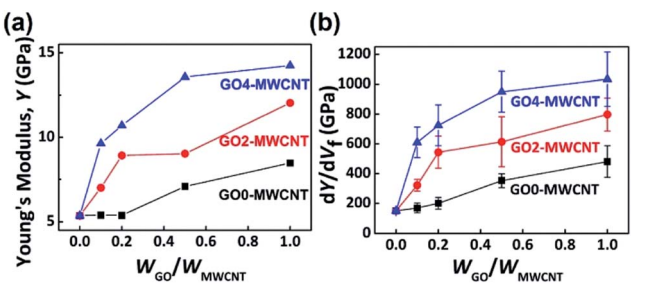

Fig. 5 Mechanical properties of GO–MWCNT/PVA composite films with different W_{GO}/W_{MWCNT}. For three composites containing different GO–MWCNT, (a) Young's modulus and (b) dY/dV_f values as a function of W_{GO}/W_{MWCNT} are plotted. The volume fraction of MWCNT was kept at 1.2%.

Table 2 Young's moduli of MWCNT/PVA composite films

	Young's modulus, Y (GPa)				
W_{GO}/W_{MWCNT}	0	1/10	1/5	1/2	1/1
PVA (unfilled)	3.4	—	—	—	—
MWCNT/PVA[b]	5.4 (58%)[a]				
GO0–MWCNT/PVA[b]	—	5.4 (58%)[a]	5.4 (58%)[a]	7.1 (108%)[a]	8.5 (149%)[a]
GO2–MWCNT/PVA[b]	—	7.0 (106%)[a]	8.9 (162%)[a]	9.0 (166%)[a]	12.0 (254%)[a]
GO4–MWCNT/PVA[b]	—	9.6 (183%)[a]	10.7 (215%)[a]	13.6 (299%)[a]	14.2 (319%)[a]

[a] Percentage values in parentheses indicate the increased degree of reinforcement by GO–MWCNT filler compared with the Young's modulus value of the pristine MWCNT. [b] The vol% of MWCNT was kept constant at 1.2%.

PVA–MWCNT composites that contained different volume fractions of MWCNT are shown in Fig. S8.†

As presented in Fig. 5 and Table 2, the pristine MWCNT increased the Young's modulus (Y) of PVA by 58% (from 3.4 to 5.4 GPa), which was comparable to the previously reported reinforcing effects of MWCNT.[45,70–73] In stark contrast to the pristine MWCNT sample, the GO–MWCNT hybrid complexes showed dramatic improvement in the mechanical properties of the PVA composites, which was, at the same time, strongly dependent on the size of the GO. For example, the GO4–MWCNT reinforced the Young's modulus of PVA by 183, 215, 299, and 319% with the W_{GO}/W_{MWCNT} of 0.1, 0.2, 0.5, and 1, respectively. In addition, over the whole range of W_{GO}/W_{MWCNT}, the highest Young's modulus was exhibited by the GO4–MWCNT, followed by the GO2–MWCNT, and GO0–MWCNT, which is the same order as the D_{MWCNT} values in Fig. 3. The Young's modulus enhancement at a given volume fraction of MWCNT (dY/dV_f) provided more apparent differences in the reinforcement efficiencies, as displayed in Fig. 5(b). Specifically, at the W_{GO}/W_{MWCNT} of 1, the dY/dV_f values were 480 GPa for the GO0–MWCNT, 797 GPa for the GO2–MWCNT, and 1033 GPa for the GO4–MWCNT, showing significant enhancement in the reinforcement efficiency by reducing the size of GO.

This enhancement of the mechanical properties of GO–MWCNT bore a resemblance to the dispersion behavior of GO–MWCNTs that was shown in Fig. 3, leading to the conclusion that the reinforcement effect by GO–MWCNT was also strongly related to the size of GO. Therefore, GO4, the smallest as well as the most efficient surfactant tested in this study, provided the largest reinforcement effect of the PVA composites at any W_{GO}/W_{MWCNT} ratio owing to its having the most homogeneously distributed MWCNTs in the PVA matrices.

Conclusions

In summary, we developed different-sized GOs from 170 to 2060 nm for dispersing MWCNTs to demonstrate the size effects of the GOs on the MWCNT dispersion, and on the electrical as well as mechanical properties of the MWCNT-based composites. The critical W_{GO}/W_{MWCNT} value for MWCNT dispersion was dramatically reduced from 0.83 to 0.14 as the size of GO decreased from 2060 to 170 nm. The minimum W_{GO}/W_{MWCNT} value required to achieve a conductive GO–MWCNT film was reduced from 0.1 to 0.025 owing to the significantly improved dispersion quality. Further investigation on the mechanical properties of the PVA–MWCNT composites showed that the reinforcement efficiency (dY/dV_f) of the GO4–MWCNT-added PVA composite was two-fold higher than that of the GO0–MWCNT-added PVA. Our investigation highlighted the importance of the size of the GO for designing and building GO–CNT-based composites with optimized electrical as well as mechanical properties for various applications, such as structural composites, transparent electrodes, and energy storage devices.

Acknowledgements

This work was supported by the KETEP and the MOTIE of the Republic of Korea (No. 20163030013620, 20163010012200). We acknowledge support by the Research Projects of the KAIST-KUSTAR and the CRH (Climate Change Research Hub) of KAIST.

References

1 J. N. Coleman, U. Khan, W. J. Blau and Y. K. Gun'ko, *Carbon*, 2006, **44**, 1624–1652.
2 S. Bal and S. Samal, *Bull. Mater. Sci.*, 2007, **30**, 379–386.
3 T. Hayashi and M. Endo, *Composites, Part B*, 2011, **42**, 2151–2157.
4 K. Song, Y. Zhang, J. Meng, E. C. Green, N. Tajaddod, H. Li and M. L. Minus, *Materials*, 2013, **6**, 2543–2577.
5 L. Hu, J. W. Choi, Y. Yang, S. Jeong, F. La Mantia, L.-F. Cui and Y. Cui, *Proc. Natl. Acad. Sci. U. S. A.*, 2009, **106**, 21490–21494.
6 D. Yu, K. Goh, H. Wang, L. Wei, W. Jiang, Q. Zhang, L. Dai and Y. Chen, *Nat. Nanotechnol.*, 2014, **9**, 555–562.
7 X. Zeng, L. Deng, Y. Yao, R. Sun, J. Xu and C.-P. Wong, *J. Mater. Chem. C*, 2016, **4**, 6037–6044.
8 J. W. Zhao, J. Chen, S. M. Xu, M. F. Shao, Q. Zhang, F. Wei, J. Ma, M. Wei, D. G. Evans and X. Duan, *Adv. Funct. Mater.*, 2014, **24**, 2938–2946.
9 M. Mao, L. Mei, L. Wu, Q. Li and M. Zhang, *RSC Adv.*, 2014, **4**, 12050–12056.
10 S. Huang, L. Li, Z. Yang, L. Zhang, H. Saiyin, T. Chen and H. Peng, *Adv. Mater.*, 2011, **23**, 4707–4710.
11 S. H. Kim, W. Song, M. W. Jung, M. A. Kang, K. Kim, S. J. Chang, S. S. Lee, J. Lim, J. Hwang, S. Myung and K. S. An, *Adv. Mater.*, 2014, **26**, 4247–4252.

12 J. H. Park, S. J. Lee, T. I. Lee, J. H. Kim, C.-H. Kim, G. S. Chae, M.-H. Ham, H. K. Baik and J.-M. Myoung, *J. Mater. Chem. C*, 2013, **1**, 1840–1845.
13 J. Garoz-Ruiz, D. Ibañez, E. C. Romero, V. Ruiz, A. Heras and A. Colina, *RSC Adv.*, 2016, **6**, 31431–31439.
14 B. P. Grady, *Macromol. Rapid Commun.*, 2010, **31**, 247–257.
15 L. Henrard, E. Hernández, P. Bernier and A. Rubio, *Phys. Rev. B: Condens. Matter Mater. Phys.*, 1999, **60**, R8521–R8524.
16 N. G. Sahoo, S. Rana, J. W. Cho, L. Li and S. H. Chan, *Prog. Polym. Sci.*, 2010, **35**, 837–867.
17 Q. Zheng and Q. Jiang, *Phys. Rev. Lett.*, 2002, **88**, 455031–455033.
18 P.-C. Ma, N. A. Siddiqui, G. Marom and J.-K. Kim, *Composites, Part A*, 2010, **41**, 1345–1367.
19 K. Balasubramanian and M. Burghard, *Small*, 2005, **1**, 180–192.
20 Y. Wang, Z. Iqbal and S. Mitra, *J. Am. Chem. Soc.*, 2006, **128**, 95–99.
21 L. Xu, Z. Ye, Q. Cui and Z. Gu, *Macromol. Chem. Phys.*, 2009, **210**, 2194–2202.
22 J. Lee, H. Yang, C. H. Park, H.-H. Cho, H. Yun and B. J. Kim, *Chem. Mater.*, 2016, **28**, 3446–3453.
23 K. Paek, H. Yang, J. Lee, J. Park and B. J. Kim, *ACS Nano*, 2014, **8**, 2848–2856.
24 H. Yang, K. Paek and B. J. Kim, *Nanoscale*, 2013, **5**, 5720–5724.
25 H. Yang, D. J. Kang, K. H. Ku, H.-H. Cho, C. H. Park, J. Lee, D. C. Lee, P. M. Ajayan and B. J. Kim, *ACS Macro Lett.*, 2014, **3**, 985–990.
26 H.-H. Cho, H. Yang, D. J. Kang and B. J. Kim, *ACS Appl. Mater. Interfaces*, 2015, **7**, 8615–8621.
27 J. D. Fowler, M. J. Allen, V. C. Tung, Y. Yang, R. B. Kaner and B. H. Weiller, *ACS Nano*, 2009, **3**, 301–306.
28 Kenry, J. C. Yeo, J. Yu, M. Shang, K. P. Loh and C. T. Lim, *Small*, 2016, **12**, 1593–1604.
29 J. T. Robinson, F. K. Perkins, E. S. Snow, Z. Wei and P. E. Sheehan, *Nano Lett.*, 2008, **8**, 3137–3140.
30 J. Kim, L. J. Cote, F. Kim, W. Yuan, K. R. Shull and J. Huang, *J. Am. Chem. Soc.*, 2010, **132**, 8180–8186.
31 Y. He, F. Wu, X. Sun, R. Li, Y. Guo, C. Li, L. Zhang, F. Xing, W. Wang and J. Gao, *ACS Appl. Mater. Interfaces*, 2013, **5**, 4843–4855.
32 J. Luo, L. J. Cote, V. C. Tung, A. T. L. Tan, P. E. Goins, J. Wu and J. Huang, *J. Am. Chem. Soc.*, 2010, **132**, 17667–17669.
33 L. Qiu, X. Yang, X. Gou, W. Yang, Z. F. Ma, G. G. Wallace and D. Li, *Chem.–Eur. J.*, 2010, **16**, 10653–10658.
34 C. Zhang, L. Ren, X. Wang and T. Liu, *J. Phys. Chem. C*, 2010, **114**, 11435–11440.
35 L. Tian, M. J. Meziani, F. Lu, C. Y. Kong, L. Cao, T. J. Thorne and Y.-P. Sun, *ACS Appl. Mater. Interfaces*, 2010, **2**, 3217–3222.
36 L. Tian, P. Anilkumar, L. Cao, C. Y. Kong, M. J. Meziani, H. Qian, L. M. Veca, T. J. Thorne, K. N. Tackett, T. Edwards and Y.-P. Sun, *ACS Nano*, 2011, **5**, 3052–3058.
37 J. Kim, L. J. Cote and J. Huang, *Acc. Chem. Res.*, 2012, **45**, 1356–1364.
38 G. Gonçalves, M. Vila, I. Bdikin, A. de Andrés, N. Emami, R. A. S. Ferreira, L. D. Carlos, J. Grácio and P. A. A. P. Marques, *Sci. Rep.*, 2014, **4**, 6735.
39 J. Ma, R. Liu, X. Wang, Q. Liu, Y. Chen, R. P. Valle, Y. Y. Zuo, T. Xia and S. Liu, *ACS Nano*, 2015, **9**, 10498–10515.
40 H. Yang, K. H. Ku, J. M. Shin, J. Lee, C. H. Park, H.-H. Cho, S. G. Jang and B. J. Kim, *Chem. Mater.*, 2016, **28**, 830–837.
41 M. Park, K. Song, T. Lee, J. Cha, I. Lyo and B.-S. Kim, *ACS Appl. Mater. Interfaces*, 2016, **8**, 21595–21602.
42 T. Kwon, T. Kim, F. b. Ali, D. J. Kang, M. Yoo, J. Bang, W. Lee and B. J. Kim, *Macromolecules*, 2011, **44**, 9852–9862.
43 K. H. Ku, H. Yang, J. M. Shin and B. J. Kim, *J. Polym. Sci., Part A: Polym. Chem.*, 2015, **53**, 188–192.
44 D. C. Marcano, D. V. Kosynkin, J. M. Berlin, A. Sinitskii, Z. Sun, A. Slesarev, L. B. Alemany, W. Lu and J. M. Tour, *ACS Nano*, 2010, **4**, 4806–4814.
45 Y. Hou, J. Tang, H. Zhang, C. Qian, Y. Feng and J. Liu, *ACS Nano*, 2009, **3**, 1057–1062.
46 J. Liang, Y. Huang, L. Zhang, Y. Wang, Y. Ma, T. Guo and Y. Chen, *Adv. Funct. Mater.*, 2009, **19**, 2297–2302.
47 L. Jiang, X.-P. Shen, J.-L. Wu and K.-C. Shen, *J. Appl. Polym. Sci.*, 2010, **118**, 275–279.
48 Y. Feng, N. Dong, G. Wang, Y. Li, S. Zhang, K. Wang, L. Zhang, W. J. Blau and J. Wang, *Opt. Express*, 2015, **23**, 559–569.
49 M. Zheng, A. Jagota, E. D. Semke, B. A. Diner, R. S. McLean, S. R. Lustig, R. E. Richardson and N. G. Tassi, *Nat. Mater.*, 2003, **2**, 338–342.
50 J. I. Paredes, S. Villar-Rodil, A. Martínez-Alonso and J. M. D. Tascón, *Langmuir*, 2008, **24**, 10560–10564.
51 J. L. Bahr, E. T. Mickelson, M. J. Bronikowski, R. E. Smalley and J. M. Tour, *Chem. Commun.*, 2001, 193–194.
52 M. D. Clark, S. Subramanian and R. Krishnamoorti, *J. Colloid Interface Sci.*, 2011, **354**, 144–151.
53 R. M. F. Fernandes, B. Abreu, B. Claro, M. Buzaglo, O. Regev, I. Furo and E. F. Marques, *Langmuir*, 2015, **31**, 10955–10965.
54 Z. Li, G. Luo, W. Zhou, F. Wei, R. Xiang and Y. Liu, *Nanotechnology*, 2006, **17**, 3692–3698.
55 P. M. Ajayan and J. M. Tour, *Nature*, 2007, **447**, 1066–1068.
56 J. Fan, Z. Shi, M. Tian, J. Wang and J. Yin, *ACS Appl. Mater. Interfaces*, 2012, **4**, 5956–5965.
57 H. Gu, S. Tadakamalla, X. Zhang, Y. Huang, Y. Jiang, H. A. Colorado, Z. Luo, S. Wei and Z. Guo, *J. Mater. Chem. C*, 2013, **1**, 729–743.
58 Y. C. Jung, D. Shimamoto, H. Muramatsu, Y. A. Kim, T. Hayashi, M. Terrones and M. Endo, *Adv. Mater.*, 2008, **20**, 4509–4512.
59 X. Zeng, S. Yu, L. Ye, M. Li, Z. Pan, R. Sun and J. Xu, *J. Mater. Chem. C*, 2015, **3**, 187–195.
60 Y. Zhang and S. Huang, *RSC Adv.*, 2016, **6**, 26210–26215.
61 S. Pande, A. Chaudhary, D. Patel, B. P. Singh and R. B. Mathur, *RSC Adv.*, 2014, **4**, 13839–13849.
62 M. J. A. Hore and R. J. Composto, *Macromolecules*, 2014, **47**, 875–887.
63 H.-J. Chung, J. Kim, K. Ohno and R. J. Composto, *ACS Macro Lett.*, 2012, **1**, 252–256.

64 H.-j. Chung, K. Ohno, T. Fukuda and R. J. Composto, *Nano Lett.*, 2005, **5**, 1878–1882.
65 D. J. Kang, T. Kwon, M. P. Kim, C.-H. Cho, H. Jung, J. Bang and B. J. Kim, *ACS Nano*, 2011, **5**, 9017–9027.
66 X. C. Chen and P. F. Green, *Langmuir*, 2010, **26**, 3659–3665.
67 S. K. Kumar, N. Jouault, B. Benicewicz and T. Neely, *Macromolecules*, 2013, **46**, 3199–3214.
68 J. F. Moll, P. Akcora, A. Rungta, S. Gong, R. H. Colby, B. C. Benicewicz and S. K. Kumar, *Macromolecules*, 2011, **44**, 7473–7477.
69 Y. Li, R. Umer, Y. A. Samad, L. Zheng and K. Liao, *Carbon*, 2013, **55**, 321–327.
70 Y. Wang, Z. Wang, P. Ma, H. Bai, W. Dong, Y. Xie and M. Chen, *RSC Adv.*, 2015, **5**, 72691–72698.
71 M. Cadek, J. N. Coleman, V. Barron, K. Hedicke and W. J. Blau, *Appl. Phys. Lett.*, 2002, **81**, 5123–5125.
72 M. Cadek, J. N. Coleman, K. P. Ryan, V. Nicolosi, G. Bister, A. Fonseca, J. B. Nagy, K. Szostak, F. Béguin and W. J. Blau, *Nano Lett.*, 2004, **4**, 353–356.
73 J. N. Coleman, M. Cadek, R. Blake, V. Nicolosi, K. P. Ryan, C. Belton, A. Fonseca, J. B. Nagy, Y. K. Gun'ko and W. J. Blau, *Adv. Funct. Mater.*, 2004, **14**, 791–798.